Volume 11. Number 1. 103-111 APRIL 2022

Jurnal ilmiah pendidikan fisika Al-Biruni
https://ejournal.radenintan.ac.id/index.php/al-biruni/index
DOI: 10.24042/jipfalbiruni.v11i1.11929

e-ISSN: 2503-023X
P-ISSN: 2303-1832

Investigation on electron contamination of LINAC at different operating voltages using particle heavy ion transport code system (PHITS)

Bilalodin[1*], Aris Haryadi [2], Yohannes Sardjono[3], Yaser Kasesaz[4]

[1,2]Department of Physics, Jenderal Soedirman University, Central Java, Indonesia
[3]Research Center for Accelerator Technology, National Research, and Innovation Agency, Indonesia
[4]Nuclear Science and Technology Research Institute, Teheran, Iran

**Corresponding Address: bilalodin@unsoed.ac.id*

Article Info

Article history:

Received: February 5, 2022
Accepted: April 25, 2022
Published: April 29, 2022

Keywords:

Dose;
LINAC;
PHITS;
Secondary electron.

ABSTRACT

Research has been carried out to investigate the occurrence of secondary electron contamination in a linear accelerator (LINAC) machine. The research was conducted in a simulation using a Monte Carlo-based simulator, namely Particle and Heavy Ions Transport code System (PHITS). The simulation of the occurrence of secondary electron contamination was carried out based on the model of the LINAC Electa head that is operated at voltages of 6, 8, 10, 15, 18, and 25 MV, using a field area of 10 X 10 cm and SSD 100 cm. The simulation results show that electron contamination occurs due to the interaction of X-ray photons with the components of the LINAC head, namely the primary collimator, flattening filter, and secondary collimator. The secondary electron contaminants generated by the LINAC head components spread through the water phantom. The higher the operating voltage, the higher the secondary electron flux produced. The secondary electron contamination dose calculated in the water phantom shows that the higher the LINAC voltage, the higher is the dose received in the phantom.

INTRODUCTION

Megavolt X-rays are high-energy X-rays. The X-ray beam can be generated by a medical Linear Accelerator (LINAC) machine through the interaction of accelerated electrons with a target (Anderson et al., 2015). The targets that are used to produce high-energy x-rays are those with high atomic numbers (high Z) such as tungsten, gold, silver, and tantalum (Vichi et al., 2020; Yeh et al., 2017). The resulting megavolt x-ray beam can be focused, directed, and uniformed using filters and collimators placed after the target (Anam et al., 2020).

However, the interaction of high energy x-rays with filters and collimators creates contaminants in the form of secondary electrons (Mesbahi, 2009). Additionally, electron contaminants are also contributed by the interaction of electrons with the target, although in a low percentage (Seif & Bayatiani, 2015; Vichi et al., 2020).

The presence of secondary electron contaminants during treatment using LINAC may damage superficial skin tissue (dermis) to the deepest skin (hypodermis) (Butson, 1998; Mazzeo et al., 2014). Increasing the dose of secondary electron contaminants on the skin can cause an erythema (Lye et al., 2010; Yadav et al., 2010), which is the appearance of reddish patches on the skin caused by dilation of blood vessels under the skin, and desquamation, namely exfoliation of the skin from the body. The most severe impact is the occurrence of

How to cite Bilalodin, B., Haryadi, A., Sardjono, Y., & Kasesaz, Y. (2022). Investigation on electron contamination of LINAC at different operating voltages using particle heavy ion transport code system (PHITS). *Jurnal ilmiah pendidikan fisika Al-Biruni*, *11*(1), 103-111.

superficial lesions, which is abnormal skin tissues that can cause cancer or tumors (Jagtap et al., 2016; Smit & du Plessis, 2015; Yani et al., 2016).

Several studies have been carried out to understand the occurrence of secondary electron contaminants. Among them is the work of Petti et al. (1983) which revealed the presence of secondary electrons in accelerator equipment. Gonzalez et al. (2017) evaluated the emergence of secondary electrons in metallic materials. The latest research was conducted by Chegeni et al. (2021), which tried to find out what parameters affect the emergence of secondary electrons in LINAC.

Several techniques were used to calculate secondary electron contaminants, including direct measurements using electron filter plates and magnetic sweepers, spectrometry, and dosimetry methods (Chegeni et al., 2021; Han et al., 2020). Another technique used is the Monte Carlo analysis and simulation method. Sadrollahi et al. (2019) using a Monte Carlo-based program, were able to determine the secondary electron energy of 0.1 MeV using a model of the Simen Premus LINAC machine. Anam et al. (2020) using the Monte Carlo BEAMnrc-based program, were able to reveal the emergence of electron contaminants and the intensity of each component on the LINAC machine.

Although several studies have been carried out to reveal the occurrence of secondary electrons, there are still few studies that reveal the occurrence of secondary electron contaminants, displaying traces of secondary electron contaminants ranging from the target to the LINAC components and phantom. This visualization is very helpful in understanding where the secondary electron contaminants actually come from. As such, efforts to reduce contaminants so as not to have a negative impact on tissue damage can be carried out adequately. Several attempts have been made to reduce the occurrence of secondary electron contaminants, including installing magnetic deflectors, replacing part of the air column between the patient and the head of the radiotherapy system with helium gas, and limiting treatment time (Chegeni et al., 2021).

Visualization of traces of electron contaminants can be displayed using the Particle and Heavy Ions Transport code System (PHITS). The advantage of the PHITS code or PHITS program is that it is a Monte Carlo-based program, equipped with a tally that can display a visualization of trace particles in 2 and 3 dimensions and calculate the physical quantity to be determined. The PHITS program is also suitable for simulating the transport of charged and uncharged particles that move randomly (Hashimoto et al., 2015). The PHITS program has been tested and become the basis for developing designs of medical devices in Japan (Furuta & Sato, 2021).

The use of the PHITS program to visualize the occurance of secondary electron contamination and the calculation of the dose generated from the LINAC machine at various voltage variations have never been done. Hence, the study is a novelty of this research.

Furthermore, the purpose of the study is to visually consider the occurrence of secondary electrons in the components of the LINAC machine and calculate the dose of secondary electrons in the water phantom using the PHITS code.

METHOD

Modeling of LINAC Device

The simulation of the LINAC device model is based on the head of the LINAC Electa model which is operated at voltages of 6, 8, 10, 15, 18, and 25 MV. The selection of voltage is based on the operating voltage of the LINAC machine usually used in the hospital. The output field area of the radiation field is set for a field area of 10 × 10 cm and a Source to Image Receptor Distance (SID) of 100 cm. At a distance of 100 cm is placed a water

phantom with a cube geometry measuring 40 × 40 × 40 cm^3 (Hasan et al., 2019).

The model of the LINAC head consists of a number of main components, namely electron source, target, primary collimator, flattening filter, and secondary collimator. The components of the LINAC device head were simulated using the Particle and Heavy Ions Transport code System (PHITS) version 3.2 program (Sato et al., 2015). The model of the components of the LINAC head and water phantom shown in Figure 1.

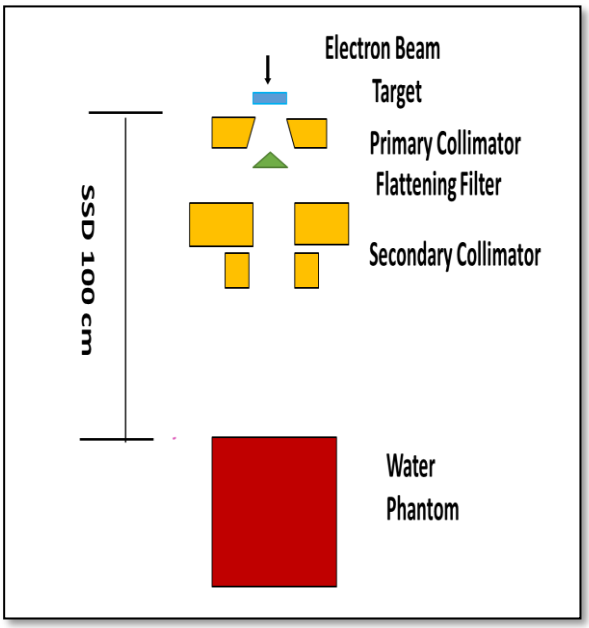

Figure 1. Configuration of LINAC head components and water phantom for investigation of electron contaminant.

The materials for the LINAC head component refer to the Electa linac model. The main components are made of metal and a mixture of several metals. The complete material data is shown in Table 1.

Table 1. Data of LINAC-head material (Abou-taleb et al., 2018)

Components of LINAC head	Material
Target	Gold (Au)
Primary collimator	Tungsten(W), Nickel (Ni), Iron (Fe)
Flattening filter	Copper (Cu)
Secondary collimator	Tungsten(W), Nickel (Ni), Iron (Fe)

Simulation of Secondary Electron Contamination

Inspection on secondary electron contaminants is carried out starting from the target to the water phantom. The spectrum and distribution of the electron particle traces were observed using a tally track. Meanwhile, the absorbed dose uses a tally deposit. The simulation LINAC machine was carried out with primary electron particles numbering to 10^9. The ANGEL software is used to display particle traces and geometry visualization. The cross-sectional data library used for electrons and photons is JENDL-4.0 (Sato et al., 2015). These data will expectedly guarantee the validity of the model designed.

RESULTS AND DISCUSSION

Validity of model

Model validation is intended to ensure that the model matches the actual X-ray equipment. The matching criteria include the equipment producing X-ray beams and the Percentage Depth Dose (PDD) curve must match the measurement results (Ezzati et al., 2020).

The simulation results show that the LINAC machine has produced X-ray beams, which is indicated by the presence of X-ray particle traces starting from the target through the collimator and up to the water phantom. Traces of high-intensity X-ray particles are shown in red and low-intensity particles are shown in blue. High-intensity X-rays are generated near the target and the lowest in the area obstructed by the components of the LINAC head. This high intensity of X-rays around the target is caused by the mechanism for the generation of X-rays between accelerated electrons and the target (Anam et al., 2020). The image of the simulation result of the X-ray particle traces from the LINAC head is shown in Figure 2a.

The model of LINAC machine has also matched the actual equipment. This is demonstrated by the correspondence of the PDD curve values generated by the

simulation with the measurement results (Figure 2b). The PDD curve has a low surface dose pattern then rises to a maximum value and decreases exponentially. Such a low dose on the surface of the water phantom is caused by the X-ray being attenuated. As the interaction of x-rays with water phantom increases in depth, ionization processes through the mechanism of the photoelectric effect, the Compton effect, and the production of pairs increase, resulting an increase in the dose and reaches the maximum value in the buildup area. The dose then decreases as the X-rays decrease in energy and flux or intensity (AL-Naqqash et al., 2018; Efendi et al., 2017).

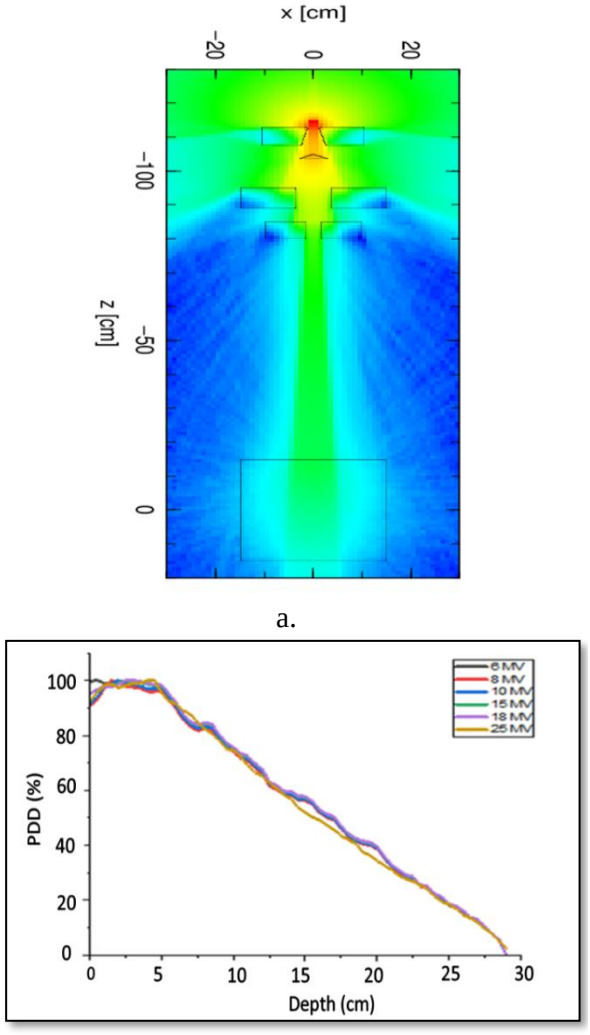

a.

b.

Figure 2. a. The simulation results of X-ray particle traces at a LINAC voltage of 8 MV. b. PDD Graph of X-Ray energy simulation results at 6,8 10, 15, 18 and 25 MV

The results of the calculation of the maximum dose build-up value on a LINAC machine operating at 6, 8, 10, 15, 18, and 25 MV show that the simulation results agree with the reference, except for the 6 MV. This difference is caused by beam hardening, that is to say beam enhancement due to scattering caused by local spots far from the radiation source (Efendi et al., 2017). The difference in the build-up value at 6 MeV is 2%. The simulation result value is still within the required tolerance (Yani et al., 2016). The simulation results of the build-up value and its comparison with the reference are shown in Table 2.

Table 2 Comparison of build-up values obtained from simulation and reference (Podgorsak, 2005)

No	Energy	Simulation	Reference	ΔL (%)
1	6 MV	1.47 cm	1.5 cm	98
2	8 MV	2.0 cm	2.0 cm	100
3	10 MV	2.5 cm	2.5 cm	100
4	15 MV	3.0 cm	3.0 cm	100
5	18 MV	3.5 cm	3.5 cm	100
6	25 MV	5.0 cm	5.0 cm	100

Secondary electron contaminants

Figure 3 shows the traces of secondary electrons resulting from the interaction of photons with components of the LINAC head operated at voltages of 6, 8, 10, 15, 18 and 25 MV. The secondary electron intensity resulting from the interaction of photons with the primary collimator, flattering filter and secondary collimator components is depicted by color intensity. The highest electron intensity is shown in red and the lowest in blue.

Based on Figure 3, the intensity of secondary electrons is highest around the primary collimator and flattering filter. The value of the electron flux intensity ranges from 10^9 to 10^{16} electrons/cm^2.s. The secondary electron intensity decreases further away from the flattering filter and

decreases further around the secondary collimator and water phantom.

Such high intensity of secondary electrons about the primary collimator is produced by the interaction between photons and W, Ni and Fe atoms through the mechanism of the photoelectric effect, Compton scattering and pair production. Based on these three mechanisms, Compton scattering is dominant (Chegeni et al., 2021). With respect to the decrease in the intensity of secondary electrons in the secondary collimator, it is due to the relatively low number of photons impinging on the component.

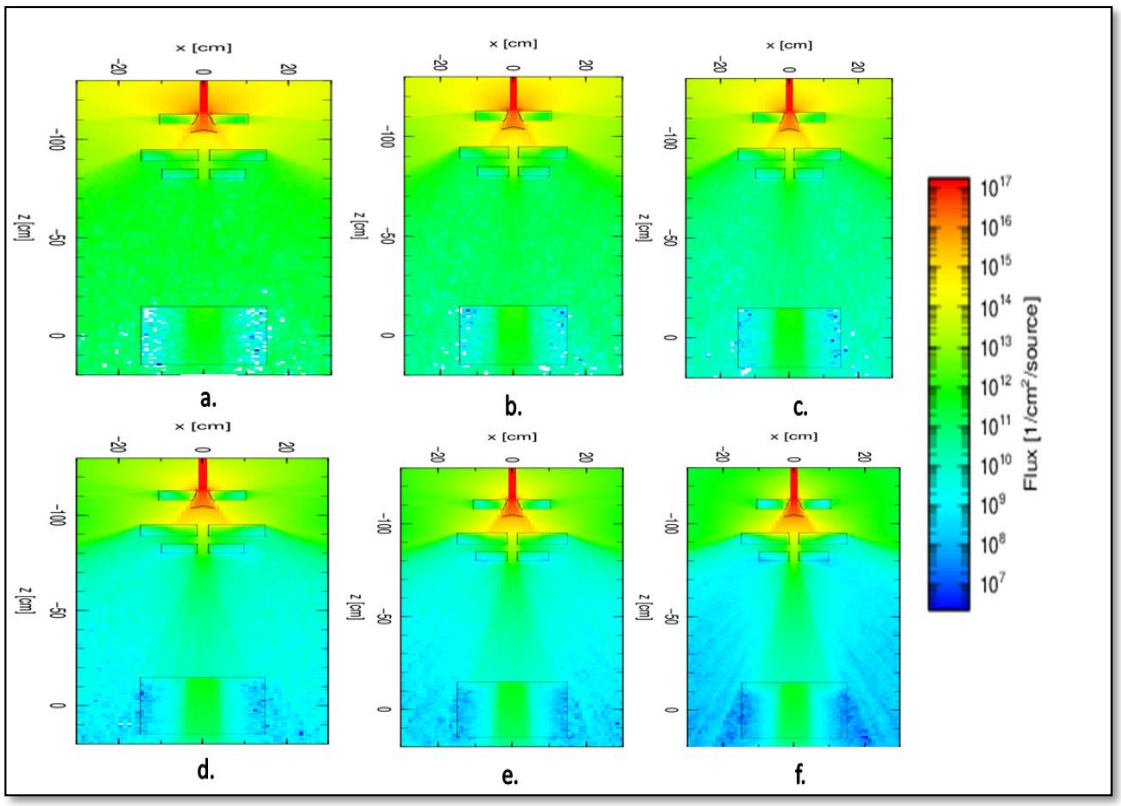

Figure 3. Particle traces of electron contaminant with X-ray voltage of (a) 6 MV, (b) 8 MV, (c) 10 MV, (d) 15 MV, (e) 18 MV, (f) 25 MV

The increase in the LINAC voltage has an impact on the electron flux intensity. The higher the voltage applied, the higher the intensity of the resulting neutron flux. An increase in voltage results in a greater primary electron velocity, such that it produces X-ray photons of higher intensity and energy when it strikes a target (Podgorsak, 2005). Subsequently, when the photon collides on the LINAC components, it also produces a higher intensity of secondary electrons. The simulation results for determining the intensity and energy distribution of secondary electrons on the water phantom surface using LINAC voltage variations are shown in Figure 4.

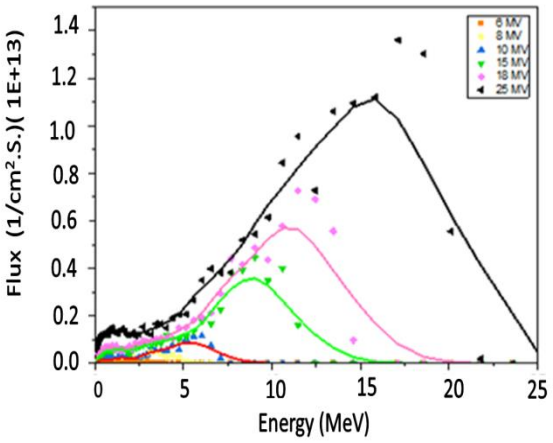

Figure 4. Spectrum of secondary electrons simulated at operating voltages of 6, 8, 10, 15, 18 and 25 MV.

Based on Figure 4 shows that the highest secondary electron flux is obtained at a voltage of 25 MV and the lowest at a voltage of 6 MV. In general, an increase in the LINAC operating voltage causes larger secondary electron fluxes. This increase is caused by the increase in the intensity of X-rays hitting the LINAC head components, such as the flattening filter and collimator (Chegeni et al., 2021; Mesbahi, 2009).

Dose of Secondary Electron Contaminant

Simulation result shows that the secondary electron flux strikes the phantom surface and penetrates further down the water phantom. The calculation results on the dose of secondary electron contamination at operating voltages of 6, 8, 10, 15, 18 and 25 MV are shown in **Figure 5**.

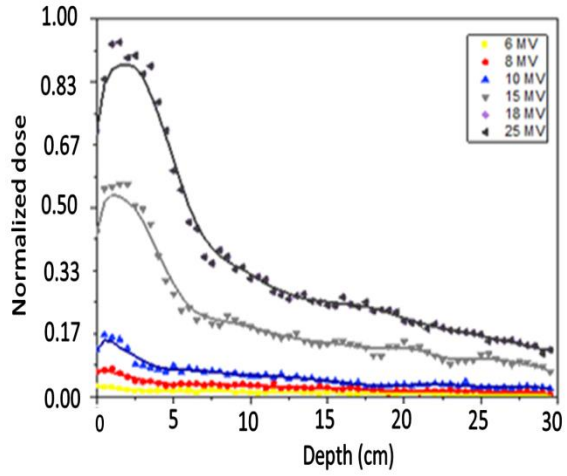

Figure 5. Dose of electron contaminants in the phantom at operating voltages of 6, 8, 10, 15, 18, and 25 MV.

Based on Figure 5 the dose on the surface of the phantom is low and increases up to certain depth, and decreases exponentially with increasing depth. At a voltage of 6, 8, and 10 MV the dose increases at a depth of, 0 cm, 0.5 cm, and 1 cm respectively. Furthermore, the maximum dose corresponding to the voltage of 15 MV occurs at a depth of 2 cm. Finally, at voltages of 18 and 25 MV, the maximum dose is reached at a depth of 1.5 cm. In general, the increase of LINAC machine voltage has an impact on the increase in the dose (Chegeni et al., 2021).

Based on the simulation results, the PHITS program has been able to accurately determine that the penetration power of secondary electron contamination occurs between 0 - 2 cm. 2 cm is the average thickness of the human skin (Oltulu et al., 2018). The presence of these contaminants causes a skin sparking effect. It is an ionization process on the skin that can cause damage to the skin (De-Colle et al., 2021; Jo et al., 2017).

CONCLUSION

An investigation has been carried out on secondary electron contaminations resulting from LINAC machine operated at voltages of 6, 8, 10, 15, 18, and 25 MV based on a validated model. The simulation results show that X-ray photons interacting with the primary collimator, flattening filter, and secondary collimator components produce secondary electron contaminants. The higher the voltage applied, the higher the secondary electron flux produced. The secondary electron contamination dose calculated in water phantom shows that dose increases with the LINAC operating voltage.

Future research is to consider other aspects that affect the occurrence of contaminants, such as the radiation field and the type of material that makes up the LINAC head.

ACKNOWLEDGMENT

We would like to thank the Institute of Research and Community Service, Jenderal Soedirman University for providing research funds.

AUTHORS CONTRIBUTIONS

BL conducted the study on the components that constitute the LINAC head, constructed a model as the basis for the simulation, wrote the code for the PHITS program, and prepared the manuscript. AH contributed to conducting simulations. YS contributed to analyzing research data. YK

edited the English manuscript. All authors read and approved the final manuscript.

REFERENCES

Abou-taleb, W. M., Hassan, M. H., Mallah, E. A. El, & Kotb, S. M. (2018). MCNP5 evaluation of photoneutron production from the Alexandria University 15 MV Elekta Precise medical LINAC. *Applied Radiation and Isotopes*, *135*(1), 184–191. https://doi.org/10.1016/j.apradiso.2018.01.036

AL-Naqqash, M. A., Essa, S. I., & Hasan, R. H. (2018). Measurement of percentage depth dose (PDD) for 6 MeV in water phantom and homogenous actual planning. *Iraqi Journal of Physics (IJP)*, *16*(37), 1–6. https://doi.org/10.30723/ijp.v16i37.70

Anam, C., Soejoko, D. S., Haryanto, F., Yani, S., & Dougherty, G. (2020). Electron contamination for 6 MV photon beams from an Elekta linac: Monte Carlo simulation. *Journal of Physics and Its Applications*, *2*(2), 97–101. https://doi.org/10.14710/jpa.v2i2.7771

Anderson, R., Lamey, M., Macpherson, M., Carlone, M., & Introduction, I. (2015). Simulation of a medical linear accelerator for teaching purposes. *Journal of Applied Clinical Medical Physics*, *16*(3), 359–377.

Butson, M. J. (1998). *Skin dose from radiotherapy x-rays*. Online University of Wollongong.

Chegeni, N., Rahim, F., Tahmasbi, M., Farzanegan, Z., & Hosseini, S. K. (2021). Measurement and calculation of electron contamination for radiotherapy photon mode. *Jundishapur Journal of Health Sciences*, *13*(1), 1–9. https://doi.org/10.5812/jjhs.115067

De-Colle, C., Nachbar, M., Mönnich, D., Boeke, S., Gani, C., Weidner, N., Heinrich, V., Winter, J., Tsitsekidis, S., Dohm, O., Zips, D., & Thorwarth, D. (2021). Analysis of the electron-stream effect in patients treated with partial breast irradiation using the 1.5 T MR-linear accelerator. *Clinical and Translational Radiation Oncology*, *27*(1), 103–108. https://doi.org/10.1016/j.ctro.2020.12.005

Efendi, M. A., Funsian, A., Chittrakarn, T., & Bhongsuwan, T. (2017). Monte carlo simulation of 6 MV flattening filter free photon beam of truebeam STx LINAC at songklanagarind hospital. *Sains Malaysiana*, *46*(9), 1407–1411. https://doi.org/10.17576/jsm-2017-4609-08

Ezzati, A. O., Studenski, M. T., & Gohari, M. (2020). Spatial mesh-based surface source model for the electron contamination of an 18 MV photon beams. *Journal of Medical Physics*, *45*(4), 221–225. https://doi.org/10.4103/jmp.JMP_29_20

Furuta, T., & Sato, T. (2021). Medical application of particle and heavy ion transport code system PHITS. *Radiological Physics and Technology*, *14*(3), 215–225. https://doi.org/10.1007/s12194-021-00628-0

Gonzalez, L. A., Angelucci, M., Larciprete, R., & Cimino, R. (2017). The secondary electron yield of noble metal surfaces. *AIP Advances*, *7*(11), 1–7. https://doi.org/10.1063/1.5000118

Han, W., Zheng, M., Banerjee, A., Luo, Y. Z., Shen, L., & Khursheed, A. (2020). Quantitative material analysis using secondary electron energy spectromicroscopy. *Scientific Reports*, *10*(1), 1–14. https://doi.org/10.1038/s41598-020-78973-0

Hasan, R. H., Essa, S. I., & AL-Naqqash, M. A. (2019). Depth dose measurement in water phantom for two X-ray energies (6MeV and 10MeV) in comparison with actual planning. *Iraqi Journal of*

Science, *60*(8), 1689–1693. https://doi.org/10.24996/ijs.2019.60.8.5

Hashimoto, S., Iwamoto, O., Iwamoto, Y., Sato, T., & Niita, K. (2015). PHITS simulation of quasi-monoenergetic neutron sources from 7Li(p,n) reactions. *Energy Procedia*, *71*(1), 191–196. https://doi.org/10.1016/j.egypro.2014.11.869

Jagtap, A. S., Palani Selvam, T., Patil, B. J., Chavan, S. T., Pethe, S. N., Kulkarni, G., Dahiwale, S. S., Bhoraskar, V. N., & Dhole, S. D. (2016). Monte Carlo based investigations of electron contamination from telecobalt unit head in build up region and its impact on surface dose. *Applied Radiation and Isotopes*, *118*(1), 175–181. https://doi.org/10.1016/j.apradiso.2016.09.012

Jo, I. Y., Kim, S. W., & Son, S. H. (2017). Dosimetric evaluation of the skin-sparing effects of 3-dimensional conformal radiotherapy and intensity-modulated radiotherapy for left breast cancer. *Oncotarget*, *8*(2), 3059–3063. https://doi.org/10.18632/oncotarget.13830

Lye, J. E., Butler, D. J., & Webb, D. V. (2010). Enhanced epidermal dose caused by localized electron contamination from lead cutouts used in kilovoltage radiotherapy. *Medical Physics*, *37*(8), 3935–3939. https://doi.org/10.1118/1.3458722

Mazzeo, E., Rubino, L., Buglione, M., Antognoni, P., Magrini, S. M., Bertoni, F., Parmiggiani, M., Barbieri, P., & Bertoni, F. (2014). The current management of mycosis fungoides and Sézary syndrome and the role of radiotherapy: Principles and indications. *Reports of Practical Oncology and Radiotherapy*, *19*(2), 77–91. https://doi.org/10.1016/j.rpor.2013.07.009

Mesbahi, A. (2009). A Monte Carlo study on neutron and electron contamination of an unflattened 18-MV photon beam. *Applied Radiation and Isotopes*, *67*(1), 55–60. https://doi.org/10.1016/j.apradiso.2008.07.013

Oltulu, P., Ince, B., Kökbudak, N., Findik, S., & Kiliç, F. (2018). Measurement of epidermis, dermis, and total skin thicknesses from six different body regions with a new ethical histometric technique. *Turkish Journal of Plastic Surgery*, *26*(2), 56–61. https://doi.org/10.4103/tjps.tjps_2_17

Petti, P. L., Goodman, M. S., Gabriel, T. A., & Mohan, R. (1983). Investigation of buildup dose from electron contamination of clinical photon beams. *Medical Physics*, *10*(1), 18–24. https://doi.org/10.1118/1.595287

Podgorsak, E. B. (2005). *Radiation oncology physics*. IAEA.

Sadrollahi, A., Nuesken, F., Licht, N., Rübe, C., & Dzierma, Y. (2019). Monte-Carlo simulation of the Siemens Artiste linear accelerator flat 6 MV and flattening-filter-free 7 MV beam line. *PLoS ONE*, *14*(1), 1–17. https://doi.org/10.1371/journal.pone.0210069

Sato, T., Niita, K., Matsuda, N., Hashimoto, S., Iwamoto, Y., Furuta, T., Noda, S., Ogawa, T., Iwase, H., Nakashima, H., Fukahori, T., Okumura, K., Kai, T., Chiba, S., & Sihver, L. (2015). Overview of particle and heavy ion transport code system PHITS. *Annals of Nuclear Energy*, *82*(1), 110–115. https://doi.org/10.1016/j.anucene.2014.08.023

Seif, F., & Bayatiani, M. R. (2015). Evaluation of electron contamination in cancer treatment with megavoltage photon beams: Monte Carlo study. *J Biomed Phys Eng 2015;*, *5*(1), 31–38.

Smit, C., & du Plessis, F. C. P. (2015). Deriving electron contamination characteristics using Monte Carlo beam data. *Physica Medica*, *31*(2015), 1–14.

https://doi.org/10.1016/j.ejmp.2015.07.126

Vichi, S., Dean, D., Ricci, S., Zagni, F., Berardi, P., & Mostacci, D. (2020). Activation study of a 15MeV LINAC via Monte Carlo simulations. *Radiation Physics and Chemistry*, *172*(1), 1–6. https://doi.org/10.1016/j.radphyschem.2020.108758

Yadav, G., Yadav, R. S., & Kumar, A. (2010). Effect of various physical parameters on surface and build-up dose for 15-MV X-rays. *Journal of Medical Physics*, *35*(4), 202–206. https://doi.org/10.4103/0971-6203.71761

Yani, S., Dirgayussa, I. G. E., Rhani, M. F., Soh, R. C. X., Haryanto, F., & Arif, I. (2016). Monte Carlo study on electron contamination and output factors of small field dosimetry in 6 MV photon beam. *Smart Science*, *4*(2), 87–94. https://doi.org/10.1080/23080477.2016.1195609

Yeh, B. M., FitzGerald, P. F., Edic, P. M., Lambert, J. W., Colborn, R. E., Marino, M. E., Evans, P. M., Roberts, J. C., Wang, Z. J., Wong, M. J., & Bonitatibus, P. J. (2017). Opportunities for new CT contrast agents to maximize the diagnostic potential of emerging spectral CT technologies. *Advanced Drug Delivery Reviews*, *113*(23), 201–222. https://doi.org/10.1016/j.addr.2016.09.001